SELECTIVE SUPPRESSION OF CARRIER-DRIVEN PHOTOCHEMICAL ETCHING: RAMAN SPECTROSCOPY AS A DIAGNOSTIC TOOL

C. I. H. ASHBY, D. R. Myers, G. A. Vawter, R. M. BIEFELD, and J. F. KLEM
Sandia National Laboratories, Albuquerque, New Mexico 87185

SAND--90-1740C

DE91 007495

ABSTRACT

Carrier-driven photochemical etching of semiconductors can be selectively suppressed by altering the near-surface region to enhance carrier recombination, thereby reducing the supply of carriers that drive the surface etching reaction. Two methods for enhancing recombination and decreasing the etch rate at a given phonon flux include ion implantation and localized Zn diffusion. Raman spectroscopy can be employed to determine whether sufficient alteration of electronic properties has occurred to suppress etching.

Carrier-driven photochemical reactions, which require direct participation of free carriers for the chemical reaction to proceed, can be selectively suppressed by increasing the minority carrier recombination rate, thereby reducing the supply of carriers that drive the surface etching reaction. Two methods for enhancing recombination and decreasing the etching quantum yield, which is the number of atoms removed per incident photon, include ion implantation and localized Zn diffusion. For ion implantation, recombination-promoting defect concentrations depend on ion species, fluence, and annealing both during and after the implantation process. Other recombination processes related to carrier scattering from ionized impurities from in-diffusion of dopants or following implant activation can control etching.

Raman spectroscopy can be employed to detect changes in electronic properties that correlate with etching suppression. Changes that occur in the LO-phonon lineshape, such as those associated with phonon confinement and ionized impurity scattering, can be diagnostic of the carrier-driven etching behavior following a specific treatment. We have demonstrated two applications of Raman spectroscopy as a diagnostic for suppression of the carrier-driven photochemical etching of GaAs.

EXPERIMENT

The substrate material for both implantation and Zn-diffusion treatments was n-GaAs (100) with an impurity concentration of $1.0\pm0.2\times10^{17}$ Si/cm^3. Samples of this material were implanted with 40-keV $^{11}B^+$ ions at fluences of 10^{10}, 10^{12}, and 10^{14} ions/cm^2. Other samples were type-converted to p ~ mid-10^{20}/cm^3 over a depth of about 1.2 μm by closed-tube Zn diffusion (1). Diffusion was performed in a sealed quartz ampoule using elemental Zn and As. Type-conversion to a lower Zn concentration (10^{17}-10^{18}/cm^3 p-GaAs) by Zn diffusion in an MOCVD reactor under an AsH_3 overpressure (2) permitted comparison of the effects of low and high p-type impurity concentrations on etching quantum yields. The lower-concentration p-GaAs was type converted over a depth of approximately 200 nm. The Raman probe depth (26 nm) was much shallowerer than the type-converted regions.

All samples were photochemically etched under conditions that produce no measurable thermal etching of an untreated n-GaAs (100) surface during a reaction time of 30 minutes. The substrate temperature was 363±4 K; the carrier-driven reaction is temperature independent in this regime. Chlorine atoms were generated in a dc glow discharge in 5% HCl in He located several centimeters upstream from the sample. More detailed descriptions of the discharge conditions and sample preparation for the ion-implanted (3) and Zn-diffused (4) samples have been reported.

Carriers were generated by absorption of 514.5-nm light from an Ar^+ laser operating in the Gaussian TEM_{00} mode. Ion-implanted samples were etched for 15 minutes at a laser power density of 680 W/cm^2. Zn-diffused samples were etched for 10 minutes at 600 W/cm^2. Quantum yields (atoms removed/incident photon) were calculated from measured etched depths by assuming that a cylinder of material with a diameter equal to the FWHM of the beam was removed.

Raman spectra were measured at room temperature in air in a backscattering geometry using 457.9-nm light that was line-focussed to an average power density less than $2W/cm^2$ to minimize contributions from sample heating. The large absorption coefficient at 457.9 nm ($1.9 \times 10^5/cm$ (5)) probes a surface depth of only $1/2\alpha \approx 30$ nm. The spectra displayed here were taken in the $x(y,y+z)\bar{x}$ polarization configuration. Polarization analysis showed all prominent features to be present only in the $x(y,z)\bar{x}$ (perpendicular) configuration; no significant features above baseline were observed in the $x(y,y)\bar{x}$ (parallel) configuration for any of the samples reported here. Signal-averaged spectra were collected using a triple monochromator with a dual-microchannel-plate optical multichannel analyzer (OMA), which had a channel-to-channel separation of 1 cm^{-1}.

RESULTS AND DISCUSSION

The steady-state concentration of holes in an n-type semiconductor is described by the 1-dimensional continuity equation for holes where the four principal contributions are diffusion, field-induced drift, carrier generation by photon absorption, and carrier loss through recombination (6). Selective etching can be achieved by controlling carrier generation, transport, and/or recombination; recombination is altered in this work to produce selective etching. The recombination lifetime, τ, can be reduced from an initial value, τ_o, by introduction of impurities (τ_{imp}) or ion-induced defects (τ_{def}).

$$1/\tau = 1/\tau_o + 1/\tau_{def} + 1/\tau_{imp} + \ldots \quad (1)$$

The recombination lifetime resulting from implantation-induced defects is given by

$$1/\tau_{def} = \frac{V_{th}\,\sigma_e\sigma_h N_t\,(pn - n_i^2)/(p-p_o)}{\sigma_p\{p+n_i\exp[(E_i-E_t)/kT]\} + \sigma_n\{n+n_i\exp[(E_t-E_i)/kT]\}} \quad (2)$$

where N_t is the defect-associated trap concentration, n_i is the intrinsic carrier concentration, n and p are the electron and hole concentrations, respectively, E_i is the intrinsic Fermi level energy, E_t is the trap energy, v_{th} is the hole thermal velocity, σ_e and σ_h are the electron and hole trapping cross sections, respectively (6).

Estimation of the degree of reaction suppression would be relatively simple if suppression depended linearly on total ion fluence. However, the dependence of quantum yield on ion fluence is sublinear, as shown in Table I. The nonlinear dependence suggests that the residual defect concentration following these ion implantations depends sublinearly on the total ion fluence. Consequently, one needs a method for determining the residual concentration of ion-induced defects if one is to predict the amount of etch suppression that a given ion fluence will produce. We have examined the potential of Raman spectroscopy to provide a measurement of this residual defect concentration.

Table I. Quantum Yields and Defect Concentrations versus Ion Fluence

Ion Fluence (B^+/cm^2)	0	10^{10}	10^{12}	10^{14}
Quantum yield (atoms/photon)	1.25±0.10	1.14±0.10	0.69±0.10	0±0.05
Calculated Defect Concentration (cm-3)				
Raman	0	0 0-2.3x10^{16}	8.8x10^{16} (3.7-12)	1.2x10^{18} (0.75-1.4)
TRIM	0	2.2x10^{16}	2.2x10^{18}	2.2x10^{20}

In undamaged GaAs, with its long-range order, the LO phonon spectrum follows the 1st-order Raman selection rule of wave vector conservation with q≈0. As the concentration of defects produced by implantion increases, the long-range order is disrupted and localized phonon modes can occur. The consequence is nonconservation of crystal momentum in the Raman process and a contribution to the 1st order LO phonon spectrum from q's for which $|q-q_0| \leq 1/2L$, where L is the phonon confinement length. A model for implantation-induced confinement (7) using a Gaussian attenuation factor gives the following expression for the Raman lineshape.

$$I(\omega) \propto \int_0^1 \exp\left(\frac{-q^2L^2}{4}\right) \frac{q^2\, dq}{[\omega-\omega(q)]^2 + [\Gamma_o/2]^2} \qquad (3)$$

We have used the phonon confinement length as a measure of the inter-defect separation; the reciprocal cube of this separation distance is used to calculate the residual defect concentration produced by implantation. The confinement length, L, for each sample was determined by calculating the lineshape for a given L using Eqn. 3, convolving the calculated lineshape with the OMA instrument response function, and comparing the calculated spectrum with the experimental spectrum. Experimental spectra and calculated spectra with their associated phonon confinement lengths are shown in Fig. 1. The defect concentrations and their associated uncertainties determined by this method are listed in Table I. The broad instrument function of the dual microchannel plate OMA used in this work leads to the large uncertainties in L that produce the range of estimated defect concentrations in Table I. Greater certainty in the lineshape and, consequently, in the derived value of L should be possible using a CCD (charge-coupled device) array or photon counting techniques.

An alternative method for estimating defect concentrations employs the Monte Carlo TRIM code to calculate the energy deposited into displacements and uses the Kinchin-Pease model to calculate displacements from energy deposition (8). The calculated damage profile shows that 13% of the total energy-into-damage is deposited in the Raman probe depth of 26 nm. The average number of displacements (defects/cm^3) in the Raman probe volume are listed in for TRIM in Table I. These values assume that each displacement produces one residual defect. The TRIM values may overestimate the number of residual defects for a number of reasons, including multiple displacements of a given atom and thermal annealing during or after implantation. Within experimental uncertainty, there is an order of magnitude agreement between the Raman and the Kinchin-Pease estimates of defect concentration at the 10^{10} B/cm^3 fluence.

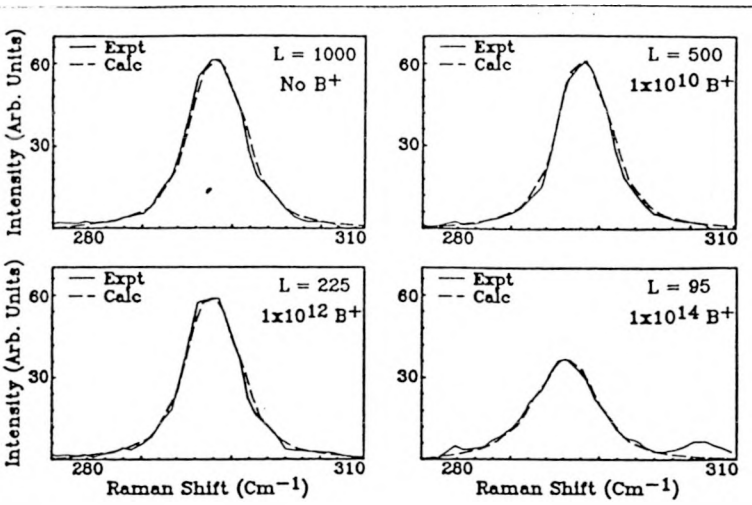

1. Raman spectra: experimental and calculated for 4 implant fluences; L in Angstroms.

The supply of holes and, consequently, the etching quantum yield will be reduced as the minority carrier lifetime is reduced by the implantation-induced defects. The model employed here assumes that the quantum yield ratio for two different fluences will be proportional to the different minority carrier lifetimes in the two materials.

We have employed Eqn. 2 to calculate hole lifetimes as a function of defect concentrations listed in Table I. The values employed in these calculations were selected in the following way. For bulk-grown GaAs, nonradiative recombination is dominant and hole lifetimes are typically of the order of 20 nsec (9). Because measured carrier lifetimes are not available for our substrate material, we assume this typical bulk hole lifetime. At the photoexcitation level employed in the etching, carrier pairs are generated at an average rate of $8 \times 10^{25}/cm^3$ within the $1/\alpha$ depth ($\alpha = 9.2 \times 10^4/cm$). Assuming a 20-nsec hole lifetime, one calculates a steady state hole concentration of $1.6 \times 10^{18}/cm^3$ during etching. A range of trap energies (E_t) that virtually spans the forbidden gap have been reported for implanted GaAs (10). However, most lie between 1.3 and 0.2 eV above the valence band; over this range, the variation in calculated hole lifetime is less than 1% at 300K. We have employed a value of 0.4 eV for E_t. Trapping cross section values are not available, so we have assumed a typical hole cross section of 1×10^{-15} cm^2 (6). For hole traps in unimplanted GaAs, the ratios of hole to electron cross section range from 10^2 to 10^{12}. We have assumed that electron trapping at implantaion-induced defects is fairly efficient and have employed an electron cross section of 1×10^{-17} cm^2. These selected values produce very good agreement between the experimental quantum yield ratio and the ratio based on the TRIM defect estimate for the for the 10^{10} B/cm^2 sample (Fig. 2). The corresponding quantum yield ratio for the Raman-derived defect concentration is also in agreement with the experimental quantum yield ratio, within experimental uncertainty.

The quantum yield ratios calculated with Eqn. 4 for the defect concentrations from TRIM and our Raman measurement are shown in Fig. 2.

$$\frac{\phi_{imp}}{\phi_o} = \frac{1}{\tau_o \left(\frac{1}{\tau_o} + \frac{1}{\tau_{def}} \right)} \qquad (4)$$

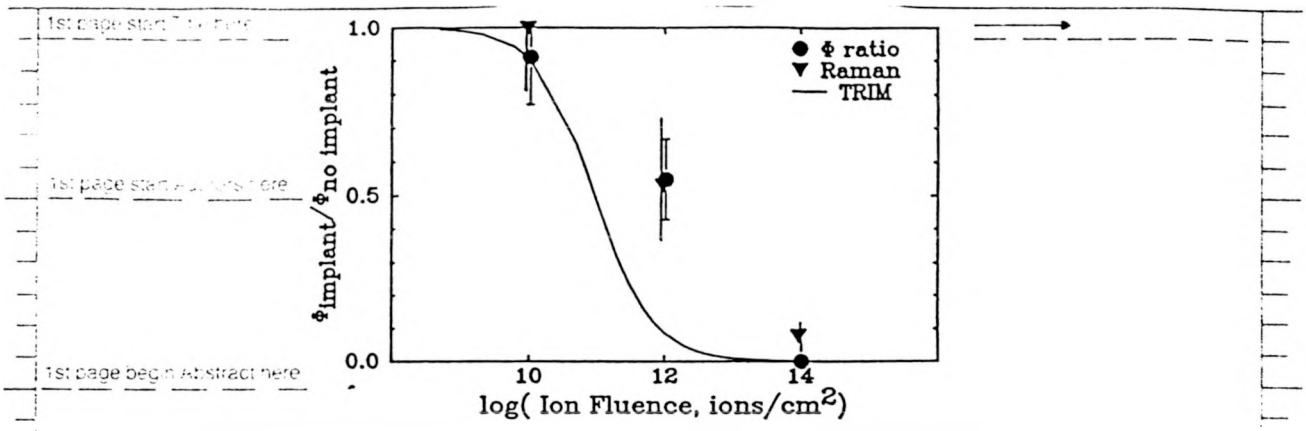

2. Comparison of etching quantum yield ratios: experimental, Raman and TRIM estimates.

The Raman-derived quantum yield ratios and the experimental ratios are in good agreement. Much poorer agreement with experiment results for the ratios derived from TRIM. Thus, it appears that defect concentrations derived from Raman spectroscopy may be a useful predictor of etching suppression by ion implantation.

Information about the differences in the electronic properties resulting from the two different Zn-diffusion techniques can also be derived from the Raman spectra. The most obvious change in the spectra following in-diffusion of Zn to the $10^{20}/cm^3$ level is the appearance of the major peak at 265 cm^{-1} and the pronounced reduction in the 292 cm^{-1} peak intensity shown in Fig. 3. The lower-energy, broader peak at 265 cm^{-1} results from the coupled LO-phonon-plasmon modes with wavevectors larger than the nominal q≈0 transfer from the photons (11). This wavevector nonconservation results from elastic scattering of the photoexcited intermediate-state holes and electrons by ionized impurities (12) introduced by the Zn diffusion. In contrast, the Raman spectrum from the Zn-diffused 10^{17} $/cm^3$ p-GaAs sample does not differ significantly from the spectrum of the original n-type substrate.

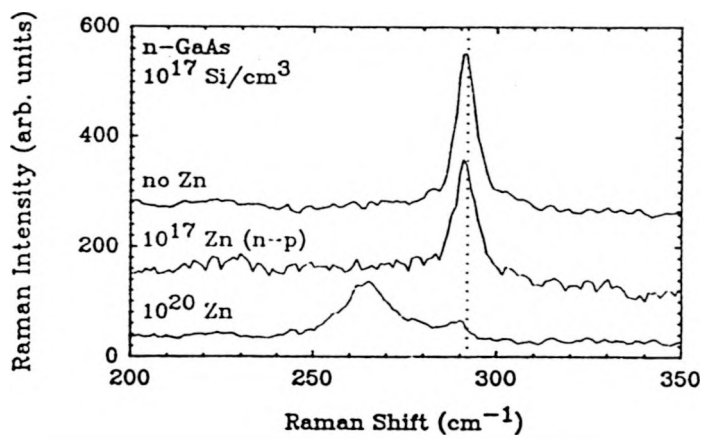

3. Raman spectra for Zn-diffused GaAs:original, type-converted, and heavily doped samples. Dotted line indicated ideal LO phonon position at 292 cm^{-1}.

The difference in the LO-phonon spectral region corresponds to significant differences in the etching behavior of the two Zn-diffused samples. Reaction suppression is observed only in those samples that display an increase in elastic scattering, as shown in Fig. 3. The Raman spectrum of the n-GaAs after type conversion to 10^{17}-10^{18} p-GaAs in the MOCVD system shows no significant increase in elastic scattering following Zn diffusion. The etching behavior of the original and this type converted

material are also virtually identical. Thus, type conversion that does not result in significant changes in the Raman spectrum also permits efficient photocarrier-driven etching. In contrast, the mid-10^{20} Zn/cm^3 material that exhibits pronounced elastic scattering effects in its Raman spectrum also has highly suppressed photochemical reactivity. Although the elastic scattering process that is detected by the Raman technique is not itself responsible for carrier loss and reaction suppression, it may be used as an indicator of the presence of adequate concentrations of impurity atoms to produce the desired suppression.

SUMMARY

Changes in LO-phonon Raman spectra can serve as a diagnostic for changes in electronic properties of GaAs that have direct consequences for carrier-driven etching. Raman spectroscopy may be useful as a pre-etch diagnostic to determine the adequacy of a particular treatment for achieving etch suppression. This approach should be applicable to both dry and wet carrier-driven processes.

ACKNOWLEDGEMENTS

The authors wish to thank J. L. Dishman, D. Moore, B. Fuch, and R. J. Granfield for technical assistance. This work was performed at Sandia National Laboratories and supported by the U.S. Department of Energy, Office of Basic Energy Sciences, under Contract No. DE-AC04-76DP00789.

REFERENCES

1. G. A. Vawter, E. Omura, X. S. Wu, J. L. Merz, L. Coldren, and E. Hu, J. Appl. Phys. 63, 5541 (1988).

2. R. M. Biefeld, G. C. Osbourn, P. L. Gourley, and I. J. Fritz, J. Electron. Mater. 12, 903 (1983).

3. C. I. H. Ashby, D. R. Myers, and F. L. Vook, J. Electrochem. Soc. 136, 782 (1989).

4. C. I. H. Ashby, D. R. Myers, G. A. Vawter, R. M. Biefeld, and A. K. Datye, J. Appl. Phys. 68, 2406 (1990).

5. D. E. Aspnes and A. A. Studna, Phys. Rev. B 27, 985 (1983).

6. S. M. Sze, Semiconductor Devices: Physics and Technology (John Wiley & Sons, New York, 1985), p. 48.

7. K. K. Tiong, P. M. Amirtharaj, F. H. Pollak, and D. E. Aspnes, Appl. Phys. Lett. 44, 122 (1984).

8. G. H. Kinchin and R. S. Pease, Repts. on Prog. in Physics 18, 1 (1955).

9. A. R. Peaker and B. Hamilton, Chemtronics 3, 194 (1988).

10. D. V. Morgan and P. D. Taylor, in Ion Implantation in Semiconductors 1976, edited by F. Chernow, J. A. Borders, and D. K. Brice, (Plenum Press, New York, 1977), p. 555.

11. D. Olego and M. Cardona, Phys. Rev. B 24 7217 (1981).

12. A. A. Gogolin and E. I. Rashba, in Physics of Semiconductors, edited by F. G. Funi, (North-Holland, New York, 1976), p. 284.